

24 COMPACT OBJECTS

24.1 Useful references

- Prialnik, 2nd ed., Ch. 10
- Choudhuri, Secs. 5.3–5.6
- Hansen, Kawaler, and Trimble, Ch. 10

24.2 Introduction

As we have discussed up to this point, mass is destiny when describing the evolution and final fates of single stars. Fig. 46 breaks down the ultimate states of stars of a range of initial masses. Furthermore, the mass of an object's final remnant (after AGB mass loss, supernova, etc.) is similarly deterministic.

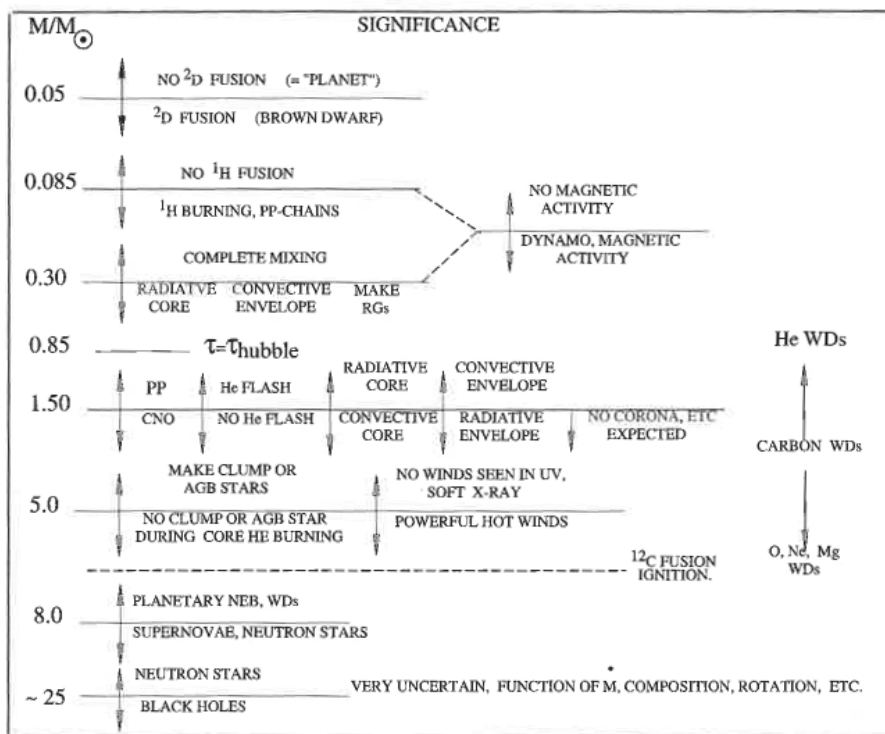


Figure 49: Mass is destiny: final fates of single stars. (Fig. 2.4 of Hansen, Kawaler, and Trimble, 2nd Ed.).

- $M_{\text{fin}} < 1.4M_{\odot}$: White dwarf, supported by electron degeneracy pressure.
- $1.4M_{\odot} < M_{\text{fin}} \lesssim 3M_{\odot}$: Neutron star, supported by neutron degeneracy pressure. The upper limit here is not known with great precision.
- $M_{\text{fin}} \gtrsim 3M_{\odot}$: No known support can hold up the remnant; it collapses into a gravitational singularity, a **black hole**.

Fig. 47 shows the masses of known stellar remnants, emphasizing that we know almost nothing about compact objects with masses between $2\text{--}5 M_{\odot}$. But before we examine these most massive of remnants, let's first reconsider white dwarfs in a bit more detail.

24.3 White Dwarfs Redux

Let's construct a more detailed model of a white dwarf than what we've managed before. For example, we've talked before about the WD equation of state and qualitatively estimated their radii, but we can do better.

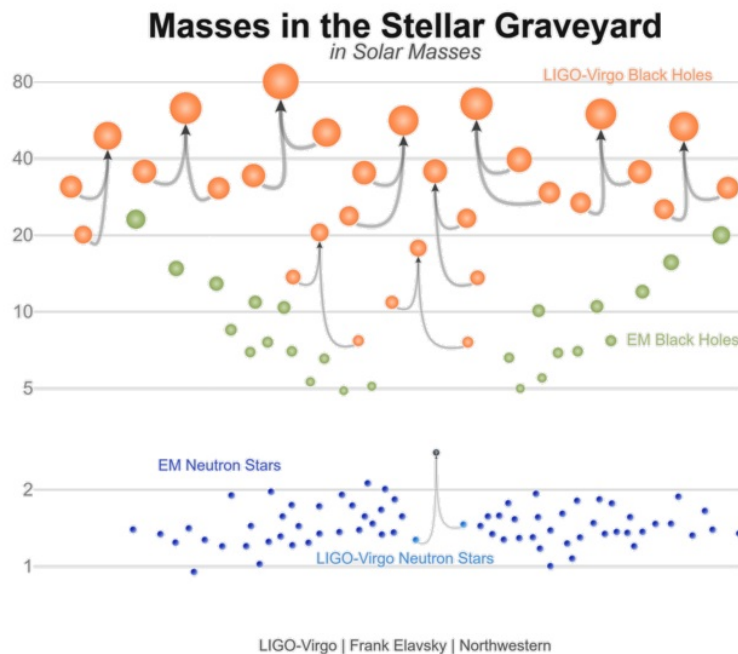


Figure 50: Masses of known extremely compact objects: black holes (above) and neutron stars (below), as of early 2019. Objects joined by arrows indicate mergers observed via gravitational waves.

White dwarf mass-radius relations

Assume we have N electrons that supply the supporting degeneracy pressure, and N protons supplying the mass. Gravity packs the particles closely together (though not as tightly as in a neutron star!). By the Heisenberg uncertainty principle,

$$(541) \quad \Delta x \Delta p \gtrsim \hbar$$

the tight constraints on position imply a correspondingly large momentum dispersion, and so the total kinetic energy will increase.

So the Fermi momentum of the electrons will be approximately

$$(542) \quad p_F \approx \frac{\hbar}{\Delta x} \approx \hbar n^{1/3}.$$

And thus the total Fermi energy will be

$$(543) \quad E_F = \sqrt{p_F^2 c^2 + m_e^2 c^4}.$$

Depending on whether or not the electrons are strongly relativistic, we will have either

(544)

$$E_{F,NR} \approx m_e c^2 + \frac{p_F^2}{2m_e}$$

(545)

$$\approx C + \frac{\hbar^2}{2m_e} \left(\frac{N}{R^3} \right)^{2/3}$$

or

(546)

$$E_{F,UR} \approx p_F c$$

(547)

$$\approx \frac{\hbar N^{1/3} c}{R} \left(\frac{N}{R^3} \right)^{2/3}$$

The total gravitational energy will be dominated by the more massive proton, and will be roughly

$$(548) \quad E_G \approx -\frac{GM^2}{R} = -N \frac{GMm_p}{R}.$$

Thus in the non-relativistic limit, the total energy of the system will be

$$(549) \quad E_{NR} \approx C + \frac{\hbar^2}{2m_e} \left(\frac{N^{5/3}}{R^2} \right) - \frac{GM^2}{R}.$$

This expression shows a clear minimum when plotted vs R (see Fig. 48) – this minimum is the equilibrium point, and corresponds to the radius at which a white dwarf is stable. This minimum radius occurs when

$$(550) \quad \frac{dE}{dR} = 0$$

$$(551) \quad -\frac{\hbar^2 N^{5/3}}{m_e R^3} + \frac{GM^2}{R^2} = 0$$

or equivalently, when

$$(552) \quad R = \frac{\hbar^2}{Gm_e m_p^{5/3} M^{1/3}}.$$

Thus a typical white dwarf with mass $1M_\odot$ will have a radius of just about $1R_\oplus$. Furthermore, note that $R \propto M^{-1/3}$ – so white dwarfs get smaller as we add more mass, as we saw in Sec. 21.4. (We already encountered this while discussing shell burning: as fusion ‘ash’ is steadily added to a core, it contracts despite its mass having increased.)

Alternatively, in the ultra-relativistic case the total energy of the white

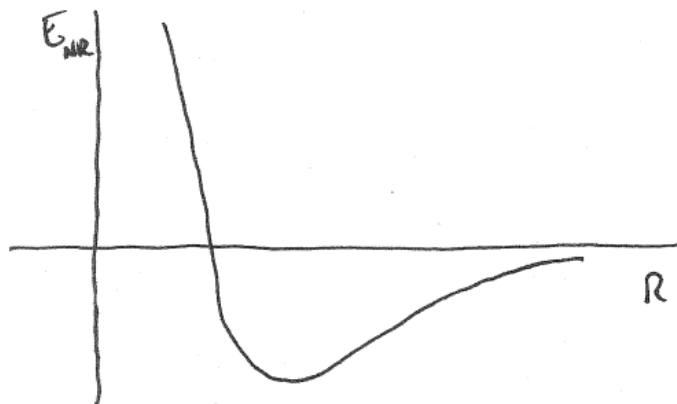


Figure 51: Total energy of a white dwarf in the non-relativistic limit (see Eq. 520). The energy minimum implies an equilibrium point: this will be the radius of the white dwarf.

dwarf will be

$$(553) \quad E_{UR} \approx \frac{\hbar c N^{4/3}}{R} - \frac{GM^2}{R}$$

$$(554) \quad = \frac{N^2}{R} \left(\hbar c N^{-2/3} - G m_p^2 \right)$$

XXXXXXXXXXXXXXXXX clarify where the above relation comes from

This expression, in contrast to Eq. 520, has no extremum with radius. So rather than a relation between mass and radius, a white dwarf in the ultra-relativistic has a single, limiting mass, given when $E = 0$:

$$(555) \quad \hbar c N^{-2/3} = G m_p^2.$$

This limiting mass is the aforementioned **Chandrasekhar Mass**, which is approximately

$$(556) \quad M_{Ch} \approx N_{max} m_p$$

$$(557) \quad \approx m_p \left(\frac{\hbar c}{G m_p^2} \right)^{3/2}$$

$$(558) \quad \approx 1.7 M_{\odot}$$

This is actually not too far off from what a further refinement would predict; we will consider this next.

Polytropic White Dwarf

The next level of refinement is to return to our polytropic model of a white dwarf, which we have discussed previously. As we've seen many times, for white dwarfs we have either

- **Non-relativistic degenerate gas:** $\gamma = 5/3, n = 3/2$.
- **Ultra-relativistic degenerate gas:** $\gamma = 4/3, n = 3$.

And as you just saw in Problem Set 7, the mass of a polytropic white dwarf is

$$(559) \quad M = 4\pi\rho_c \lambda_n^3 \zeta_{surf}^2 \left. \frac{d\phi_n}{d\zeta} \right|_{\zeta_{surf}}$$

where

$$(560) \lambda_n \left[\frac{(n+1)K\rho_c^{1-n/n}}{4\pi G} \right]^{1/2}$$

and where ξ_{surf} is the Lane-Emden surface coordinate, introduced in Sec. 17.

This means that we have either

$$M \propto \rho_c^{1/2} \text{ (for } n=3/2\text{), or}$$

$$M \propto \rho_c^0 = \text{const (for } n=3\text{)}$$

and so the mass will steadily increase up to some maximum value, as shown in Fig. 49. To find the transition point and calculate the maximum mass, we need more details. Of particular import is the polytropic constant K_{UR} . The full equation of state turns out to be

$$(561) P = \left(\frac{3}{\pi}\right)^{1/3} \frac{hc}{8m_p^{4/3}} \left(\frac{\rho}{\mu_e}\right)^{4/3}$$

which leads to a more accurate version of the Chandrasekhar Mass,

$$(562) M_{Ch} = 1.4M_{\odot} \left(\frac{\mu_e}{2}\right)^{-2}.$$

Observations of White Dwarfs

The observational history of white dwarfs is much messier – possibly even more complicated than solving polytropic equations of state. Observations established the existence of unusual celestial objects, but their natures weren't known for some time.

We now know that the first white dwarf was identified in 1783 by William Herschel. He noticed a dim companion to the $V = 4.4$ mag star 40 Eri. The colors of the faint companion indicated that it must be hot (we know now it's $\sim 10^4$ K, hotter than 40 Eri), but it is 5 mag fainter. Thus it must be tiny.

Another, similar object was identified four-score years later; this was Sirius B, discovered using a telescope in Cambridgeport, Massachusetts. Its gravitational connection to Sirius was quickly recognized, and using the tools dis-

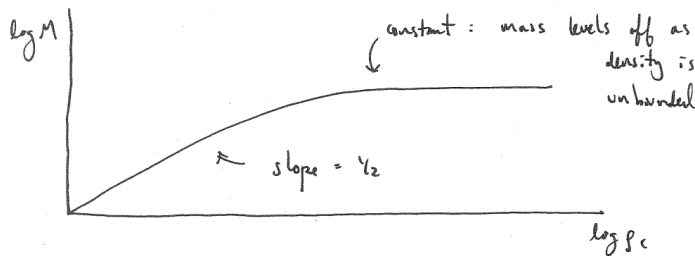


Figure 52: Mass of a white dwarf as its central density increases.

cussed in Sec. 7.3 its mass, luminosity, and (after a “high-contrast” spectrum was obtained in 1915) its temperature were all measured. These indicated $M \approx M_\odot$, $T_{\text{eff}} \approx 25,000$ K, and $R \approx 0.01R_\odot$ — implying $\rho \approx 10^6$ g cm⁻³.

These numbers were nonsense according to 19th century astrophysics. Quantum mechanics was needed to understand such a bizarre object. It wasn’t until 1926 that electron degeneracy pressure was described, and only in 1931 did Chandrasekhar identify his eponymous mass limit. Even so, conservative astronomers resisted for many years.

Other bibs and bobs about white dwarfs:

- As discussed in Sec. 21.7, the final composition of a white dwarf depends on its formation history. If it reached the 3α process, it should be carbon-oxygen. Otherwise, it’s probably just a helium white dwarf. (There may be a chance to have O-Ne-Mg WDs, but there’s no strong empirical evidence.)
- Some white dwarfs pulsate, permitting asteroseismology to more precisely determine their interior structure from the Fourier spectrum of oscillation modes.
- Gravitational redshifts have been measured from some stars. Since a photon’s energy as it leaves a gravitational well changes by

$$(563) \quad \Delta E = hv\Delta\Phi_g/c^2 = hv\frac{GM}{c^2} \left(\frac{1}{\infty} - \frac{1}{R_{WD}} \right)$$

one can measure the wavelength/frequency/energy of a known line relative to its expected location

$$(564) \quad \frac{\Delta E}{E} = -\frac{GM_{WD}}{R_{WD}c^2}$$

and so directly measure the WD’s mass-to-radius ratio.

- As has been alluded to before, white dwarfs gradually cool down on cosmic timescales. By modeling this, we can estimate the ages of individual (isolated) WDs and also of star clusters. WDs in globular clusters provided one of the first signs that the universe was >10 Gyr old!
- Analysis of white dwarf spectra reveals rotational broadening due to short rotation periods of just ~ 1000 s, as well as strong magnetic fields of $\sim 10^6$ G (from Zeeman splitting).

24.4 White Dwarf Cooling Models

White dwarfs start out extremely hot as the cores of giant stars, but once the stellar envelope is ejected they cool down: first rapidly, then slowly.

White Dwarfs: The Simple Model

In the simplest model of white dwarf cooling, the WD is an isothermal object radiating at temperature T , and its total internal energy is the kinetic energy

of its constituent particles. Thus the total energy available to the WD is

$$(565) \quad E_{tot} \approx NkT = \frac{M}{m_p} kT$$

and its luminosity is

$$(566) \quad L = -\frac{dE_{tot}}{dt} = 4\pi R^2 \sigma T^4.$$

Since the white dwarf is degenerate we will assume that its radius is constant throughout its evolution. Then we have

$$(567) \quad -\frac{M}{m_p} k \frac{dT}{dt} = 4\pi R^2 \sigma T^4$$

which, after some algebraic manipulation, yields

$$(568) \quad -T^{-4} dT = \frac{4\pi R^2 \sigma m_p}{Mk} dt$$

Thus

$$(569) \quad -\int_{T_{hot}}^T T'^{-4} dT' = \int_0^t \frac{4\pi R^2 \sigma m_p}{Mk} dt'$$

where the temperature starts at T_{hot} at $t = 0$ and evolves from there.

The solution is

$$(570) \quad \frac{3}{T^3} - \frac{3}{T_{hot}^3} = \frac{4\pi R^2 \sigma m_p}{Mk} t$$

but because of the rapid cooling, the second term is negligible after a very short time. So after further rearranging, we have

(571)

$$T(t) = \left(\frac{3Mk}{4\pi R^2 \sigma m_p} t \right)^{1/3}$$

(572)

$$= 5600 \text{ K} \left(\frac{R}{R_\oplus} \right)^{-2/3} \left(\frac{M}{M_\odot} \right)^{1/3} \left(\frac{t}{1 \text{ Gyr}} \right)^{-1/3}$$

This isn't crazy, but it isn't terribly accurate either (and its predicted $L(t)$ will be even further off). We can do better by considering a two-component WD model: the degenerate object remains the same, but its outermost veneer must have sufficiently low density that it is non-degenerate; this outer layer acts like an insulating blanket and slows heat loss from the nearly isothermal interior. Finally, we'll assume that the transition from degenerate to non-degenerate occurs at a transition radius r_{tr} .

The pressure must be continuous at r_{tr} ; recall from Eq. 431 that the condition for this transition is

$$\rho_{\text{tr}} \approx 750 \text{ g cm}^{-3} \mu_e \left(\frac{T}{10^7 \text{ K}} \right)^{3/2}.$$

So the polytropic and ideal-gas equations of state must be equal:

(573)

$$K' T_{\text{tr}}^{1+n} = \rho_{\text{tr}} \frac{k}{\mu} T_{\text{tr}}$$

(574)

$$\approx 2 \times 10^{-8} \mu_e \frac{k}{\mu} T_{\text{tr}}^{1+3/2}$$

If we assume that the envelope opacity follows Kramer's Law (Eq. 226),

$$\kappa \approx 4 \times 10^{25} \rho T^{-7/2} \text{ cm}^2 \text{ g}^{-1}$$

then the polytropic coefficient becomes

$$(575) \quad K' \approx 8 \times 10^{-15} \mu^{-1/2} \left[\frac{M/M_{\odot}}{L/L_{\odot}} \right]^{1/2}$$

for $n = 3.25$. The result is

$$(576) \quad \frac{L}{L_{\odot}} \approx 7 \times 10^{-29} \mu \frac{M}{M_{\odot}} T_{\text{tr}}^{7/2}.$$

How does this two-layer white dwarf evolve with time? The specific heat of a mixed (degenerate+ideal gas) is

$$(577) \quad c_V = \frac{3N_A k}{2\mu_I}$$

where μ_I is the mean molecular weight of the ions. So the energy output will then be

$$(578) \quad L = -\frac{dE_{\text{ions}}}{dt} = -c_V M \frac{dT_{\text{tr}}}{dt}.$$

The final solution to all this (see Iben & Tutukov 1984) is

$$(579) \quad \frac{L}{L_{\odot}} = \left(\frac{A}{12} \right)^{-7/5} \left(\frac{\mu}{2} \right)^{-2/5} \left(\frac{M}{M_{\odot}} \right) \left(\frac{t}{9 \text{ Myr}} \right)^{-7/5}.$$

This is the **Mestel cooling model** for white dwarfs – not the latest state-of-the-art, but not too bad either. Note that since we have $L \propto t^{-7/5}$ and we know $L \propto T^4$, this implies $T \propto t^{-7/20}$ — remarkably close to the power of $1/3$ we found in our simple model in Eq. 543.

In practice, a number of other factors beyond radiative considerations will

24. COMPACT OBJECTS

affect white dwarf cooling. E.g., see the *Physics Today* article on the course website about crystallization effects.

25 NEUTRON STARS

If a stellar remnant exceeds the Chandrasekhar mass, then even fully relativistic electron degeneracy pressure will be insufficient to support it. As we discussed in Sec. 23.4, only neutron degeneracy pressure can possibly halt its final and inevitable collapse. Let's now consider the astrophysics of neutron stars in more detail.

25.1 Neutronic Chemistry

For starters: why don't all the neutrons just decay away? An isolated neutron undergoes the decay

$$(580) \quad n \rightarrow p + e^- + \bar{\nu}_e$$

because

$$(581) \quad (m_n - m_p)c^2 = 1.3 \text{ MeV}.$$

The excess energy will be carried away by the electron and antineutrino.

But in a degenerate medium, the Fermi energy may exceed this 1.3 MeV limit. When this happens, there are no accessible low-energy states for the electron to occupy after decay – so the neutron decay is suppressed (alternatively, imagine the neutron decays but it is energetically favorable for the new electron to immediately recombine with an available proton). We expect this beta-decay suppression to set in when

$$(582)$$

$$E_F \gtrsim (m_n - m_p)c^2 = 1.3 \text{ MeV}$$

$$(583)$$

$$\sqrt{p_F^2 c^2 + m_e^2 c^4} \gtrsim (m_n - m_p)c^2$$

$$(584)$$

$$m_e c^2 \left(\frac{p_F^2}{m_e^2 c^2} + 1 \right)^{1/2} \gtrsim (m_n - m_p)c^2.$$

So to keep the neutrons around, the Fermi momentum must satisfy

$$(585) \quad p_F \gtrsim m_e c \left[\left(\frac{m_n - m_p}{m_e} \right)^2 - 1 \right]^{1/2}$$

or roughly $p_F c \gtrsim 1.2 \text{ MeV}$. In terms of density, we refer to Eq. 418,

$$p_F = \left(\frac{3n^3 \rho}{8\pi m_p} \right)^{1/3}.$$

So combining this with Eq. 556 we see that neutron decay is suppressed for

$$(586) \quad \rho \gtrsim 10^7 \text{ g cm}^{-3}.$$

As ρ_c reaches and exceeds this critical density, the neutron star establishes an equilibrium between neutrons, protons, and electrons. One can develop a Saha-like equation (recall Sec. 12.4) relating the populations of each type of particle; see Sec. 2.6 of Shapiro & Teukolsky for further details. Above the critical density, the so-called **neutron drip** sets in and neutrons slowly leave the individual nuclei. In the extreme end case, the star is indeed entirely neutrons.

25.2 Tolman-Oppenheimer-Volkoff

Note also that for neutron stars,

$$(587) \quad \frac{GM}{rc^2} \approx 0.1 - 0.3$$

and so we are definitely in a range where Newtonian gravity alone will not suffice. General relativity must be used instead.

Recall from Sec. 9 that gravity determines the geometry of spacetime, so that the interval (or distance) ds between two events is

$$(588) \quad ds^2 = g_{\mu\nu} dx^\mu dx^\nu$$

where $g_{\mu\nu}$ is the metric and dx^μ is the coordinate displacement between two events (see Eqs. 67 and 69).

For a spherical, static body, general relativity shows that the appropriate metric is

$$(589) \quad ds^2 = -e^{2\Phi(r)/c^2} (cdt)^2 + \frac{dr^2}{1 - 2GM/rc^2} + r^2(d\theta^2 + \sin^2\theta d\phi^2)$$

where as usual

$$(590) \quad M(r) = \int_0^r 4\pi(r')^2 \rho(r') dr'$$

and

$$(591) \quad \frac{d\Phi}{dr} = -\frac{G[M(r) + r\pi r^2 P(r)/c^2]}{r(r - 2GM(r)/c^2)}.$$

The boundary conditions are that

$$(592)$$

$$e^{2\Phi/c^2} = 1 - \frac{2GM}{rc^2} \quad (r > R_*)$$

$$(593)$$

$$\rho(r) = 0 \quad (r \geq R_*)$$

These equations build in the relativity of distance and time, plus the fact that all forms of energy (including pressure) contribute to gravity. Ultimately the new, relativistic equation of hydrostatic equilibrium is

$$(594) \quad \frac{dP}{dr} = - \left(\frac{G}{r^2} \right) \left[\frac{M + 4\pi r^3 P/c^2}{1 - 2GM(r)/rc^2} \right] \left[\rho + P/c^2 \right].$$

This is the **Tolman-Oppenheimer-Volkoff equation** (or TOV). Note that in the limit of low densities and pressures, all terms with $1/c^2$ drop out and we recover Eq. 239,

$$\frac{dP}{dr} = - \left(\frac{G}{r^2} \right) M\rho = -\rho g.$$

25.3 Neutron star interior models

To make a neutron star model, we need to solve the TOV equation – but we also need to have an equation of state to work with. The trouble is that neutron stars push us into a regime where the physics is not accurately known! But we can still consider a few limiting cases.

The first of these is to assume that the neutron star equation of state is so stiff that it is incompressible, i.e., $\rho(r) = \rho_0 = \text{constant}$. Then (as Problem Set 8 demonstrates),

$$(595) \quad P(r) = \rho_0 c^2 \left[\frac{(1 - R_S r^2/R_*^3)^{1/2} - (1 - R_S/R_*)^{1/2}}{3(1 - R_S/R_*)^{1/2} - (1 - R_S r^2/R_*^3)^{1/2}} \right]$$

where R_* is the radius of the neutron star and

$$(596) \quad R_S = \frac{2GM}{c^2}$$

is the **Schwarzschild radius**. This incompressible model shows that $P(r = 0) \rightarrow \infty$ if R_* is too small (i.e., if the NS is too compact). The denominator of Eq. 566 must be > 0 , so we obtain the constraint that

$$(597) \quad R_* > \frac{9}{8} R_S = 2.25 \frac{GM}{c^2}.$$

The implication is that a star more compact than this cannot be supported even by infinite pressure; it will collapse instead.

In reality, no fluid can be truly incompressible, since this would require an infinite (and super-luminal) sound speed. Rhoades & Ruffini (1974) developed as stiff a NS model as possible that was still consistent with relativity. Their result was that neutron stars must have $M < 3.2M_\odot$.

25.4 A bit more neutron star structure

More typically in modern studies, one chooses an equation of state – or at least, builds up $P(\rho)$ based on your favorite knowledge/assumptions about

dense matter. One picks a central density (informed by your previous model, perhaps) and integrates Eq. 565 until $P = 0$ is reached; this is the surface. One tabulates M_* and R_* for different equations of state; Fig. 50 shows the range of possible models.

Inspection of Fig. 50 shows that predicted radii and maximum masses vary by $\sim 50\%$ for neutron stars. Typical models (plotted in black) assume “normal” nuclear matter – just standard neutrons at low densities, but at higher densities condensations of hyperons, kaons, pions, etc. may all become important. Different models make different choices for when various mesons (and other particles) play a role. Until the critical density is reached, these models scale roughly as $R_* \propto M_*^{-1/3}$ (as we saw for white dwarfs in Sec. 24.3) since the stars are still explained decently well by straightforward degeneracy calculations.

Another family of models assumes that (under other assumptions) neutron stars may be composed of so-called strange quark matter. These objects would instead be hypothetical condensates of up, down, and strange quarks that would be more stable than normal matter at the high densities involved. In grossly simplified terms, these models amount to a uniform density fluid – so $R_* \propto M_*^{1/3}$.

There are also several forbidden regions:

- **General Relativity:** If a neutron star is to avoid becoming a black hole, it must always satisfy $R > 2GM/c^2$.
- **Causality:** This is the requirement that the soundspeed c_s must satisfy $dP/d\rho = c_s < c^2$.
- **Rotation:** Neutron stars rotate (like stars and other stellar remnants). To

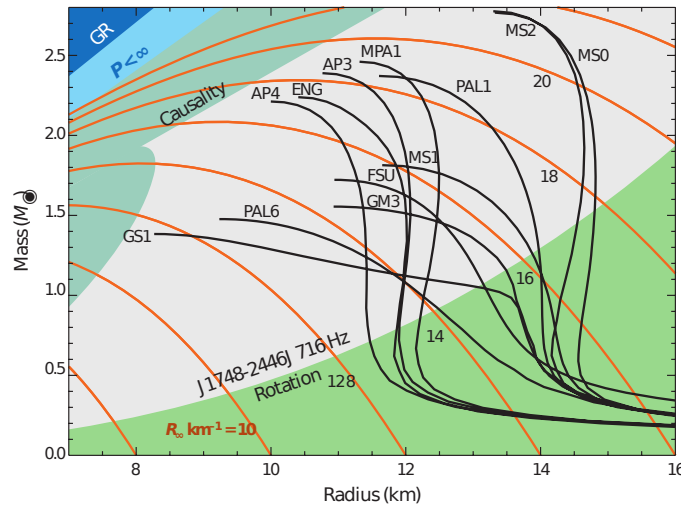


Figure 53: Predicted masses and radii (black curves) for various suggested neutron star equations of state. Orange curves show contours of $R_\infty = R(1 - 2GM/Rc^2)^{-1/2}$. Adapted from Lattimer (2012), *Ann. Rev. Nuc. Part. Sci.*.

hold together, they must satisfy

$$(598) \quad \omega^2 R < \frac{GM}{R^2}$$

or equivalently

$$(599) \quad \omega^2 < \frac{GM}{R^3}$$

and so a spinning neutron star must always satisfy

$$(600) \quad G\rho_{\text{avg}} \geq \frac{3\omega^2}{4\pi}.$$

Thus the “rotation” line corresponds to constant average density. In Fig. 50, the particular line plotted corresponds to the fastest-known rotation rate for any neutron star, $f = \omega/2\pi = 716$ Hz.

The orange curves in Fig. 50 indicate lines of constant **radiation radius** R_∞ . In principle one could observe the thermal (typically X-ray) spectrum of a young neutron star of known distance, assume a blackbody, and estimate the radius directly. But for such massive, compact objects general relativistic effects will come into play: the temperature, size, and so luminosity observed at large distances are not the “true” values that would be observed in the neutron star’s rest frame. In particular, the radiation radius is

$$(601) \quad R_\infty = R_*(1 + z_g)$$

where z_g is the **gravitational redshift** (see Eq. 534). Similarly, the temperature that will be inferred is

$$(602) \quad T_{\text{eff}}^\infty = \frac{T_{\text{eff}}}{1 + z_g}.$$

25.5 Neutron Star Observations

Neutron stars are fairly unique among objects discussed thus far. Planets, stars, nebulae, and galaxies were all observed for millennia before the true natures of these objects were uncovered. In contrast, neutron stars (along with black holes) were discussed theoretically long before any observational evidence was found.

Unfortunately the observational measurements are frustratingly sparse. Even the fastest spin rates don’t much push the physical limits. As far as maximum masses go, Fig. 47 shows that most measured NS masses are around $1.4M_\odot$. The few especially massive examples ($M_* \gtrsim 2M_\odot$) do help kill quite a few models, though. And for radii it’s worse: while some masses are measured to $\lesssim 2\%$, there are no comparably precise NS radius measurements (despite many efforts). Anyway, only ~ 10 neutron stars are close enough that we can study their thermal emission (in X-rays; $kT \gtrsim 50$ keV) — if they are more than $\gtrsim 500$ pc away then the ISM absorbs most of the radiation; and even when

detections are made, detailed atmospheric modeling (with many unknowns) is needed to accurately infer radii.

Most observational data of neutron stars come from **pulsars** – neither truly pulsating nor truly stars, but rapidly-rotating neutron stars that emit periodic radio (or other EM) emission. These were first discovered in 1967 by Jocelyn Bell, a 2nd year graduate student.

25.6 Pulsars

First discovered in 1967, thousands of pulsars are now known (see Fig. 51). Most are detected in radio, but a subset are also seen in X-rays and even gamma rays. The period of the EM emission ranges from as long as 10 s in a few cases to just 1–2 ms at the other extreme.

It was recognized almost immediately that these objects must be very small. E.g., the Crab nebular pulsar (the remnant of SN 1054) has a period of $P = 33$ msec, implying a maximum diameter of

$$(603) L \lesssim cP = (3 \times 10^5 \text{ km s}^{-1})(0.033) \approx 10^5 \text{ km}.$$

The size is consistent with a white dwarf but the period isn't. From Eq. 570

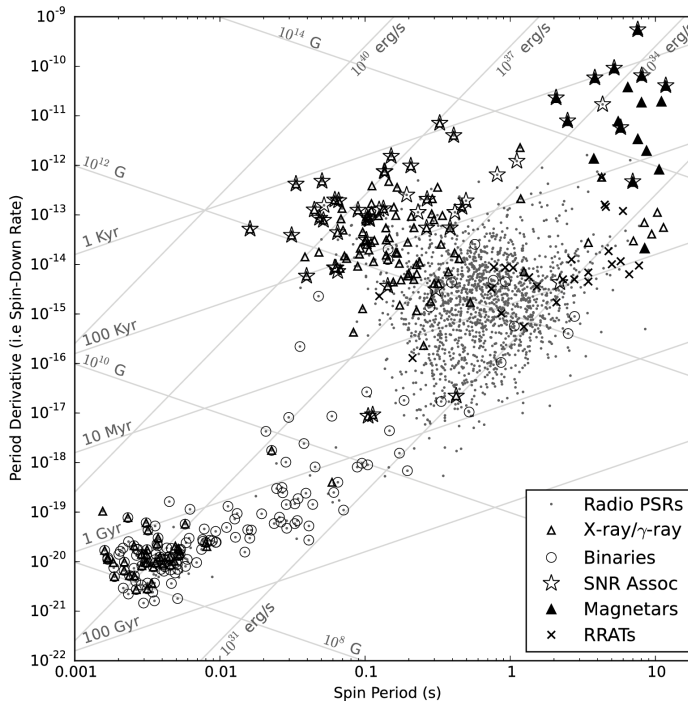


Figure 54: Pulsar observations in the traditional $P-\dot{P}$ plane. Straight lines indicate characteristic ages, spin-down luminosities, and maximum magnetic field strengths. (from <https://www.cv.nrao.edu/~sransom/web/Ch6.html>).

a white dwarf spinning that fast couldn't hold together, and the timescale for pulsations (whether freefall, Eq. 245, or sound-crossing, Eq. 248) shouldn't be lower than a few seconds. And a black hole shouldn't have any surface with which to anchor coherent, precisely-repeatable EM radiation. Thus by process of elimination, a neutron star is the most likely culprit.

The phenomenological view is that an intense beam of EM radiation is misaligned with the neutron star's rotation axis. This presumably arises from a magnetic dipole misaligned with the NS's spin axis; nonetheless many details remain unclear, and pulsar emission mechanisms remain an active area of research. But it must somehow involve a rotating magnetic field generating a large electric field from equator to pole. This in turn accelerates electrons and generates synchrotron radiation that is highly coherent and highly polarized.

Rotation and Magnetic Fields

To explain the observed emission requires rapid rotation and an extremely strong magnetic field; both can be understood from basic conservation principles. As noted previously, white dwarfs typically have $P_{WD} \sim 1000$ s and $B \sim 10^6$ G (the Earth and Sun both have magnetic fields of just ~ 1 G). Assuming angular momentum is conserved during the collapse from white dwarf to neutron star, then we should expect

$$(604) \quad I_{WD}\Omega_{WD} = I_{NS}\Omega_{NS}$$

and so

$$(605) \quad \frac{P_{NS}}{P_{WD}} = \frac{M_{NS}R_{NS}^2}{M_{WD}R_{WD}^2} \sim (10^{-3})^2.$$

Thus we should expect

$$(606) \quad P_{NS} \sim 10^{-6}P_{WD} \sim 10^{-3} \text{ sec}$$

which is roughly consistent with the shortest periods seen in Fig. 51.

As for the strong magnetic field, that can also be inferred from the known field strengths of white dwarfs. Magnetohydrodynamics tells us that magnetic flux Φ_B is conserved through any surface moving with a plasma. Thus the magnetic flux through a loop enclosing solid angle $\Delta\Omega$ around either the WD progenitor or NS progeny should be

$$(607) \quad \Phi_B = B_{WD}\Delta\Omega R_{WD}^2 \approx B_{NS}\Delta\Omega R_{NS}^2$$

and so

$$(608) \quad \frac{B_{NS}}{B_{WD}} \approx \left(\frac{R_{WD}}{R_{NS}}\right)^2 \approx 10^6.$$

Thus, we expect neutron stars to have surface magnetic field strengths of order 10^{12} G.

These strong magnetic fields induce an electromagnetic "backreaction,"

slowing the rotation over time. Unlike most stellar objects, which are in quasi-steady state, this spindown is precisely measured in many pulsars. The traditional value is the time derivative of the period, or \dot{P} (i.e., P -dot), a dimensionless quantity plotted as the vertical axis of Fig. 51. Because neutron stars spin down we almost always see $\dot{P} > 0$ (i.e., spin period increasing). Occasionally some neutron stars will show transitory “glitches” indicating sudden rearrangements of their moments of inertia (like a spinning ice skater rearranging their limbs). Glitches are usually seen in young, relatively hot neutron stars whose interiors are still stabilizing and reaching a more stable equilibrium.

When P and \dot{P} are plotted against each other as in Fig. 51, we obtain the observational equivalent of the HR diagram – but for neutron stars. The periods span a range of $10^{-3} - 10$ s, with a peak near 0.5 s; meanwhile \dot{P} has a much broader range, from $10^{-20} - 10^{-10}$ with a peak near 10^{-15} . For the lowest values of \dot{P} , the emission from these pulsars is more stable than the most precise atomic clocks (which have comparable stabilities of $\sim 10^{-16}$).

Pulsar luminosity

Fig. 51 also lets us estimate the energy loss rate of pulsars. Assuming that their energy reservoir is mainly rotational kinetic energy, then (in the classical approximation)

(609)

$$E_{\text{rot}} = \frac{1}{2} I \omega^2$$

(610)

$$= 2\pi^2 \frac{I}{P^2}$$

(611)

$$\approx \frac{4\pi^2}{5} M \left(\frac{R}{P} \right)^2$$

and so

(612)

$$\frac{dE}{dt} = \frac{d}{dt} \left(\frac{1}{2} I \omega^2 \right)$$

(613)

$$= I \omega \dot{\omega}$$

(614)

$$= \frac{8\pi^2}{5} M \frac{R^2}{P^3} \dot{P}.$$

For the Crab Nebula ($P = 33$ ms, $\dot{P} \sim 10^{-13}$, $M_* \approx 1.5M_\odot$, $R_* \approx 10$ km) we find

$$(615) \quad L = -\frac{dE}{dt} \approx 10^{38} \text{ erg s}^{-1}$$

which is comparable to the bolometric luminosity of the entire Crab Nebula; pulsars essentially convert their rotational energy into light. (Also, note that this power far outstrips the Solar luminosity of $L_{\odot} \approx 4 \times 10^{33} \text{ erg s}^{-1}$).

The mechanism of that radiation, as previously noted, is the strong, rapidly rotating magnetic field. For a given magnetic moment m , the magnetic equivalent of the Larmor formula gives the emitted power as

$$(616) \quad P = \frac{2|\ddot{m}|^2}{3c^3}.$$

Following Rybicki & Lightman (pp. 323–324), the surface magnetic field is

$$(617) \quad B_0 = \frac{2m}{R^3}.$$

The component of \vec{m} along the rotation axis is constant; given an angle α between the rotation and magnetic dipole axes,

$$(618) \quad |\ddot{m}| = \omega^2 |\vec{m}| \sin \alpha.$$

Thus the total radiated power is

$$(619) \quad L = \frac{\sin^2 \alpha}{6c^3} B_0^2 \omega^4 R^6.$$

Setting Eqs. 585 and 590 equal to each other, we see that

$$(620) \quad B_0^2 \propto P \dot{P}$$

and so the P - \dot{P} diagram of Fig. 51 should allow us to directly estimate the magnetic field strength of a pulsar. Typical values are $10^8 - 10^{15} \text{ G}$; objects with the strongest fields are termed **magnetars**. These sometimes exhibit huge outbursts, affecting terrestrial satellites and modifying the Earth's ionosphere from kpc away.

Pulsar ages and the braking index

Most importantly, the combination of P and \dot{P} allows us to estimate the age of a pulsar. If we assume that the spindown rate depends on the current spin rate to the n^{th} power, then

$$(621) \quad \dot{\omega} = a\omega^n.$$

If we fold in information about the second derivative,

$$(622) \quad \ddot{\omega} = an\omega^{n-1}\dot{\omega},$$

then

$$(623) \quad \dot{\omega}\ddot{\omega} = an\omega^n\dot{\omega}^2$$

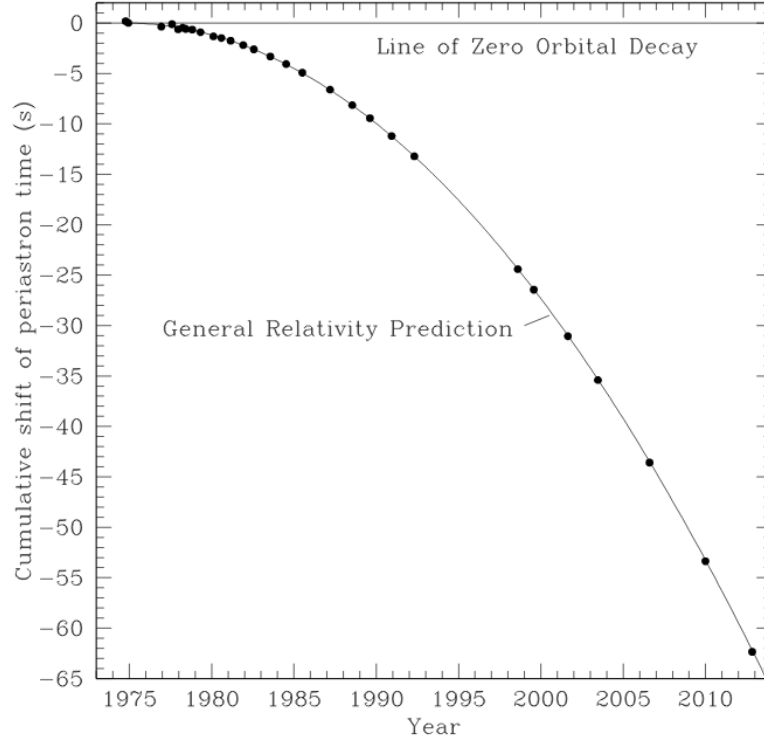


Figure 55: Period evolution of the famous Hulse-Taylor pulsar, with $P = 7.75$ hr.

and so

$$(624) \quad n = \frac{\omega \ddot{\omega}}{\dot{\omega}^2}$$

is defined as the **braking index** of the pulsar. For magnetic dipole radiation as described by Eqs. 585 and 590, we have

$$(625) \quad I\omega\dot{\omega} \propto \omega^4$$

and so the braking index $n = 3$ for pure magnetic dipole radiation.

Traditionally, one then models the period evolution as

$$(626) \quad P(t) = ct^{1/(n-1)}$$

which yields

$$(627) \quad \dot{P} = \frac{c}{n-1} t^{1/(n-1)-1} = \frac{P}{t(n-1)}$$

and so the **characteristic age** of a pulsar is given by

$$(628) \quad \tau_{\text{pulsar}} = \frac{1}{n-1} \frac{P}{\dot{P}} = \frac{P}{2\dot{P}} \quad (\text{for } n = 3).$$

Note from Eq. 597 that τ_{pulsar} actually corresponds to the time for the period to increase by a factor of two. Nonetheless it's a pretty good age indicator: for the Crab pulsar ($P = 33 \text{ ms}$, $\dot{P} = 4.2 \times 10^{-13}$) we find $\tau = 1200 \text{ yr}$. Since this pulsar formed in SN 1054, our estimate is in pretty good agreement.

As seen for the Crab, characteristic ages are only approximate. Note from Fig. 51 that many millisecond pulsars have inferred ages $> 10 \text{ Gyr}$, older than the universe! These are thought to have massively spun up by accreting high-angular-momentum material that inspiraled from a neighboring star (note that almost all ms pulsars are in binary systems). For other stars, the ages seem reasonable but the measured braking index (from P , \dot{P} , and \ddot{P}) is not 3.0 – for example, $n_{\text{crab}} = 2.515 \pm 0.005$. This reflects the fact that the radiation is only approximately dipolar.

Other tidbits, bibs, and bobs about pulsars:

- **Binary neutron stars.** When one (or both) of the objects in a binary is a neutron star, we can use the variations in the pulse arrival times to precisely map the orbit. Fig. 52 shows 40 years of data on the Hulse-Taylor pulsar, indicating inexorable inspiral of the binary due to emission of gravitational radiation. These provide excellent tests of GR, and also provide some of the most precise NS masses known.
- **Pulsar planets.** A diminutive, multibody of binary pulsars. It is not commonly known that the first confirmed planets beyond the Solar system were discovered by pulsar timing measurements. These revealed a three-planet system with orbital periods of 25, 66, and 98 days and masses of 0.02 (!), 3.9, and 4.3 M_{\oplus} , respectively. These have withstood the test of time, but they are not representative of the general population of extra-solar planets. Only ~ 6 such planets are known, in 3–4 systems.

26 BLACK HOLES

26.1 Useful references

- Kippenhahn, Weiger, and Weiss, 2nd ed., Ch. 39

26.2 Introduction

We've almost completed our astrophysical survey of stars, their evolution, and the final end products. Just to recap:

Initial Mass	Fate	Final Mass
$\lesssim 13M_{\text{Jup}}$	Planet	same
$\sim 13M_{\text{Jup}} - \sim 0.08M_{\odot}$	Brown dwarf	same
$\lesssim 0.08M_{\odot}$	Brown dwarf	same
$0.08M_{\odot} - 0.8M_{\odot}$	Lives on MS for $> t_{\text{Hubble}}$	same
$0.8M_{\odot} - \boxed{7M_{\odot}}$	White dwarf	$0.6M_{\odot} - 1.4M_{\odot}$
$\boxed{7M_{\odot}} - \boxed{20M_{\odot}}$	Neutron star	$1.4M_{\odot} - \underline{3M_{\odot}} (?)$
$\gtrsim 20M_{\odot}$	Black hole	$\gtrsim \underline{3M_{\odot}} (?)$

In this table, initial masses in boxes are uncertain due to poorly understood aspects of mass loss during stellar evolution. On the other hand, final masses that are underlined above are uncertain because the equation of state of neutron stars is only poorly known. But at final masses $\gtrsim 3M_{\odot}$, no known physics provides a pressure that can hold up a star. The increase in pressure itself is ultimately self-defeating: it gravitates! Eventually the point is reached where support would require infinite pressure; nothing can hold it up. General relativity tells us that it must collapse, leaving a black hole behind.

26.3 Observations of Black Holes

Like neutron stars, the concept of black holes was invented before any observational evidence arose. Even 18th-century natural philosophers considered the impact of sufficient gravity on corpuscular light (i.e., photons). Relativity put the discussion on firmer and more accurate footing, but decades passed before the impact of event horizons, rotating black holes, etc. were recognized. In the last half-century observers have steadily built up a catalog of objects that are

- **Massive** — i.e., $> 3M_{\odot}$ and so more massive than any plausible neutron star equation-of-state can support;
- **Compact**
- **Dark.**

This catalog includes many objects of masses $M \sim 5 - 25M_{\odot}$ (stellar remnants; see Fig. 47), along with objects with $M \sim 10^6 - 10^9M_{\odot}$ (**supermassive black holes**) at the centers of our and other galaxies. Evidence for **intermediate-mass black holes** remains inconclusive despite considerable searches.

Many of the first such stellar-mass black holes were discovered as bright X-ray sources. One of the earliest was Cygnus X-1 (i.e., the brightest X-ray source in the constellation Cygnus), over which Steven Hawking lost a bet with Kip Thorne. Another was V404 Cygni (a variable star in the same constellation), identified earlier but which underwent a massive outburst in 2015 – at peak brightness, the system was $50\times$ brighter than the Crab Nebula (supernova remnant) in X-rays. In all these systems, the X-rays arise from hot gas (at millions of K) in an accretion disk spiraling down into the black hole. Most of these systems are binaries, and the accreting material is stripped from a “normal” star (pre-collapse, pre-supernova) by the black hole. Thus the component masses can be measured using the tools discussed in Sec. 7.

For V404 Cyg, the binary mass function (Eq. 62) is

$$(629) \quad f_m = \frac{(M_X \sin I)^3}{(M_X + M_c)^2} = 6.26 \pm 0.31 M_\odot.$$

The companion star is a K giant with $M \sim M_\odot$, implying that

$$(630) \quad M_X \sin^3 I \sim 6.3 M_\odot$$

and so

$$(631) \quad M_X \gtrsim 6.3 M_\odot.$$

However, from the binary period ($P = 6.4$ d) we find only that

$$(632) \quad a \gtrsim 0.12 \text{ AU}$$

which is far larger than the Schwarzschild radius for a black hole of this mass. Thus it was some time before evidence for V404 Cyg’s black hole nature was widely accepted.

Observational evidence for supermassive black holes came initially from the velocity dispersion of stars near the centers of nearby galaxies. More recently, unambiguous evidence for these beasts came from orbital monitoring of stars around Sagittarius A* (in the Milky Way, $M \sim 4 \times 10^6 M_\odot$) and an image of the accretion disk and black hole shadow in the center of M87 ($M \sim 6 \times 10^9 M_\odot$); both are shown in Fig. 53.

26.4 Non-Newtonian Orbits

In general, sufficient evidence for a black hole requires demonstrating that too much mass is in too small of a volume, such that the mass must be enclosed within one Schwarzschild radius:

$$(633) \quad R_S = \frac{2GM}{c^2}.$$

But another key sign can be orbits with strongly non-Keplerian features that encode the nature of strong (relativistic) gravity.

Recall that the Keplerian two-body problem (Sec. 2) can be reduced to a

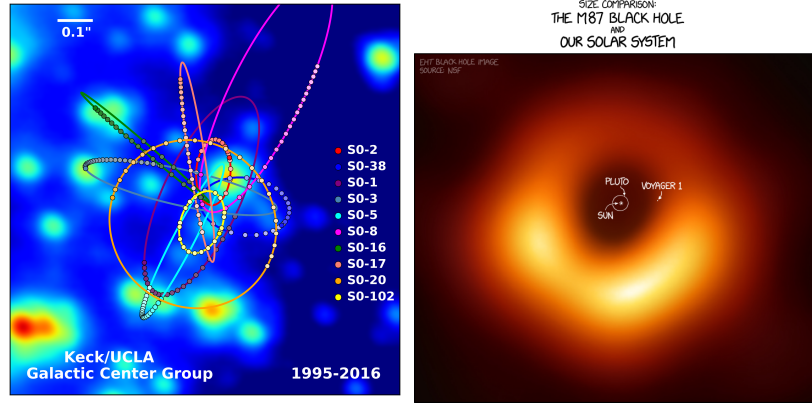


Figure 56: *Left*: Stellar orbits around Sgr A*, the supermassive black hole at the center of the Milky Way. Star S0-2 has a period of 16 yr, while other orbits are longer-period. (From <http://www.astro.ucla.edu/~ghezgroup/gc/>). *Right*: Accretion disk and shadow of the supermassive black hole at the center of nearby galaxy M87. The bright ring's diameter is $42\mu\text{as}$, or $\sim 2000\times$ smaller than the scale bar at *left*.

one-dimensional effective potential:

$$(634) \quad E = \frac{1}{2}m \left(\frac{dr}{dt} \right)^2 + \frac{L^2}{2mr^2} - \frac{GMm}{r}$$

or

$$(635) \quad \epsilon = \frac{1}{2}\dot{r}^2 + \frac{l^2}{2r^2} - \frac{GM}{r}$$

$$(636) \quad = \frac{1}{2}\dot{r}^2 + V_{\text{eff}}$$

where ϵ and ℓ are the energy and angular momentum per mass, respectively. Fig. 54 recalls this scenario, with different values of ϵ corresponding to unbound, elliptical, or circular orbits.

The equivalent for orbits in general relativity looks more interesting. If we have a non-spinning black hole, then

$$(637) \quad \left(\frac{dr}{dt} \right)^2 = \frac{\epsilon^2}{c^2} - \left(1 - \frac{2GM}{rc^2} \right) \left(c^2 + \frac{\ell^2}{r^2} \right)$$

where ϵ and ℓ have the same meanings (but ϵ now includes the full relativistic energy, including rest mass energy). But one can again define a relativistic

effective potential,

$$(638) \quad V_{\text{eff,rel}} = \left(1 - \frac{2GM}{rc^2}\right) \left(c^2 + \frac{\ell^2}{r^2}\right).$$

For a particular value of ϵ^2 , the orbital dynamics are determined by $V_{\text{eff,rel}}$ (analogously to the Newtonian case). Fig. 54 compares this case to the classical Keplerian case. A few interesting features that distinguish this new scenario:

- Circular orbits still exist if ϵ^2 is tangent to and just touches V_{eff} at a local minimum.
- Now there is an extra “hump” in the profile whose height depends on ℓ . This means that for certain values of ℓ^2 , no local minimum exists – and thus in these cases there are no stable circular orbits.
- If ϵ is high enough for a given ℓ , the trajectory can reach $r = 0$ (this never happens in the classical case for nonzero angular momentum). This is a singularity: here tidal forces become infinitely strong, and anything approaching it will be shredded.

The local minimum disappears for

$$(639) \quad \ell = \sqrt{12} \frac{GM}{c}$$

which corresponds to a stable circular orbit at $r = 3R_s$. We therefore expect no orbits inside of this radius. So even inside an accretion disk, we should have

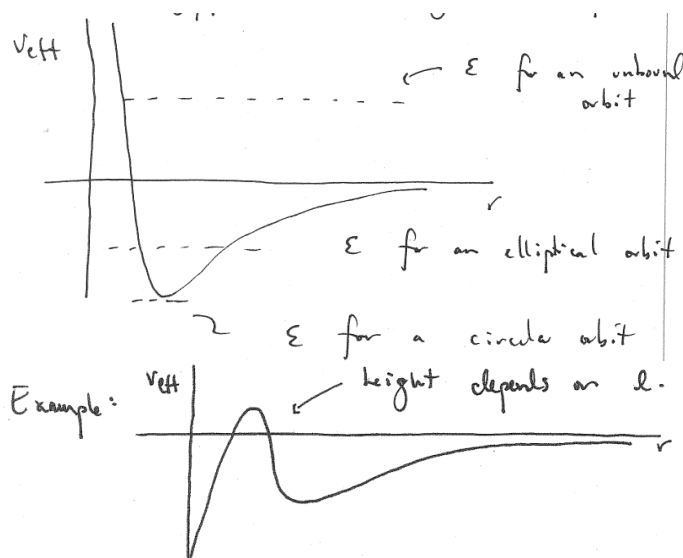


Figure 57: Effective potential vs. separation. *Top*: in a classical, Keplerian two-body system; *Bottom*: in the relativistic limit.

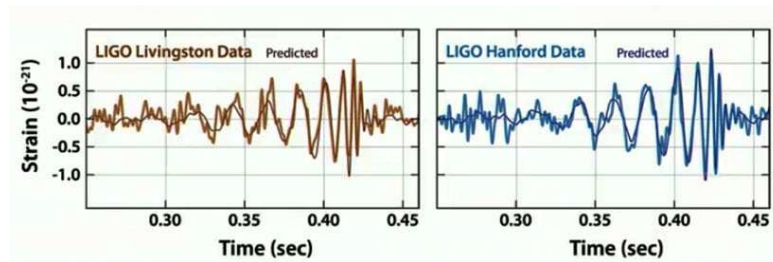


Figure 58: Gravitational wave event GW150914, indicating the inspiral and merger of two black holes.

a hole a few times larger than any black hole’s event horizon.

Note that things get even more exciting once we bring rotation into the picture. The spin of a black hole has several interesting effects:

- The event horizon changes size and shape
- Orbits have a much more complicated (non-spherical) potential.
- Orbital frequencies become affected by “frame-dragging” as the spinning black hole twists spacetime around itself.

Thanks to the **no-hair theorem**, it turns out that everything about a black hole (including the orbits around it) can be described by just three parameters: mass, angular momentum (spin), and electric charge.

26.5 Gravitational Waves and Black Holes

Black holes must solve the Einstein equations in vacuum, $G_{\mu\nu} = 0$. This is true even if two black holes are close together. In this case, they emit gravitational waves – potentially with a much higher GW luminosity than the neutron star binaries whose inspiral also indicates GW emission (Sec. 25.6). It wasn’t until the mid-2000s that computational relativity calculations first predicted what happens when two black holes orbit each other. The result, later spectacularly verified by gravitational wave measurements (see Fig. 55) includes three epochs:

1. **Inspiral:** Long before the merger, the binary is on a nearly-periodic orbit - but energy is being lost due to GW emission, so the semimajor axis (and period) steadily shrinks. Motion here is determined by the effective potential $V_{\text{eff,rel}}$, but with ϵ and ℓ slowly evolving.
2. **Plunge and Merger:** As the gravitational field grows in strength, eventually the orbits become unstable and the binary members rapidly come together, forming a single object.
3. **Ringdown:** A few, last oscillations are seen as the merged remnant settles down to the exact Kerr solution for a rotating black hole (enforcing the no-hair theorem).

This structure matches most of the gravitational wave events found so far (see e.g. Fig. 47). *Only* a black hole model, including all the necessary (very!) strong gravity physics, is able to explain these observations.